(Ba,Sr)TiO_3 ferroelectric thin films for tunable microwave applications

Wontae Chang*, Steven W. Kirchoefer, J.A. Bellotti, and J.M. Pond
Naval Research Laboratory, 4555 Overlook Avenue SW, Washington DC 20375, USA
** e-mail: chang@estd.nrl.navy.mil*

D.G. Schlom and J.H. Haeni
Department of Materials Science and Engineering, Penn State University, University Park, PA 16802, USA

Recibido el 1 de diciembre de 2003; aceptado el 28 de enero de 2004

The dielectric properties of ferroelectric thin films were investigated for tunable microwave applications. We have observed that epitaxially grown $Ba_{1-X}Sr_XTiO_3$ (BST, $0.4\leq X\leq 1$) films are distorted from the normal cubic symmetry of the corresponding bulk at room temperature. This structural distortion caused by film strain has a strong impact on the microwave dielectric properties. For compressive strain, the dielectric constant and tuning were decreased and the films showed high dielectric Q. However for tensional strain, the opposite effect was observed. This observation has been interpreted based on phenomenological thermodynamics and strain-induced polarization physics. Two experimental examples, strain-relieved films and strain-enabled films, are presented to show how film strain affects the tunable microwave properties.

Keywords: Ferroelectrics; thin films; tunable application; microwave

En el presente trabajo se investigan las propiedades dieléctricas de las películas delgadas ferroeléctricas por medio de aplicaciones de microondas sintonizables. Hemos observado que la película de $Ba_{1-X}Sr_XTiO_3$ (BST, $0.4\leq X\leq 1$) que crece epitaxialmente sufre una distorsión a partir de su simetría cúbica normal a temperatura ambiente. Esta distorsión estructural causada por el esfuerzo aplicado en la película tiene un impacto importante en sus propiedades dieléctricas. En el esfuerzo de compresión, la constante dieléctrica disminuyó y las películas mostraron un Q dieléctrico alto. No obstante, en el esfuerzo de tensión se observó el efecto contrario. Esta observación ha sido interpretada en base a la termodinámica fenomenológica y a la física de polarización inducida por tensión. Se presentan dos ejemplos experimentales, uno en películas libres de esfuerzos y otro en películas en tensión, y se muestra como la presencia de esfuerzos modifican las propiedades de sintonía en microondas.

Descriptores: Ferroeléctricos; películas delgadas; microondas.

PACS: 77.55.+f; 77.22.-d; 68.55.-a; 81.15.-z

1. Introduction

The dc electric field dependent dielectric constant of ferroelectric thin films, such as $Ba_{1-X}Sr_XTiO_3$ (BST, $0\leq X\leq 1$), is currently being used to develop high dielectric Q ($= 1/\tan\delta$) tunable microwave devices, such as voltage-controlled oscillators, tunable filters and phase shifters[1-3]. Current tunable technologies based on ferrites or semiconductors are unable to meet future system requirements for reliable, affordable, small, lightweight microwave applications with variable frequency characteristics mainly because of high power consumption, low switching speed (*i.e.*, ferrites), and low unloaded Q and nonlinear signal distortion (*i.e.*, semiconductors). Understanding the unique electronic properties of thin-film ferroelectrics as they pertain to microwave device applications, such as low dielectric loss and large tunability of the dielectric constant, is essential to develop miniature, low voltage, low-distortion microwave devices with frequency-variable transfer characteristics wideband applications. This research focuses on determining relationships between ferroelectric thin-film microstructure and microwave electronic properties resulting in an enabling tuning technology for future radar, communications, and EW systems.

Strain is one of the important factors affecting the ferroelectric properties because the strain is directly coupled with the ionic polarization in a ferroelectric[4-7]. It has been demonstrated that strain affects the ferroelectric phase transition, the dielectric constant, and the dielectric tuning[8-13]. For compressive strain, the ferroelectric phase transition peak shifts to a lower temperature, resulting in decreased dielectric constant and tuning, whereas for tensional strain, the opposite effect is observed. In this article, the film structure and microwave dielectric properties for strain-relieved BST films and highly strained $SrTiO_3$ films are analyzed and characterized for room temperature tunable microwave applications.

2. Experiment

$Ba_{0.6}Sr_{0.4}TiO_3$ (BST) thin films ($\sim$3000Å-thick) have been deposited onto (100) MgO single crystal substrates at 750°C in an oxygen ambient pressure of 200 mTorr by pulsed laser deposition (PLD) under three different processing conditions;

i) without a buffer layer,
ii) with a nominal 200Å-thick BST buffer layer, and
iii) with a nominal 600Å-thick BST buffer layer.

The thin ($\leq$ 1000Å-thick) BST buffer layer was deposited on (100) MgO substrate at room temperature and 200 mTorr O_2 by PLD. The microstructure of the BST buffer layer can be modified into any phase, from a nearly amorphous phase to a randomly oriented fully crystalline phase, depending on the in-situ heat treatment following the room temperature deposition. The output of a short-pulsed (30 ns full-width at half-maximum) KrF excimer laser (λ=248 nm) operating at a repetition rate of 5 Hz was focused to a spot size of $\sim$0.1 cm^2 and an energy density of $\sim$1.9 J/cm^2 onto $Ba_{0.6}Sr_{0.}4TiO_3$

ceramic target. The vaporized material was deposited onto a substrate approximately 5 cm away from the target. All the deposited films were post-annealed in flowing O_2 at 1000°C for 6 hours.

$SrTiO_3$ thin films of various thicknesses (100, 200, 300, 500, and 1000Å-thick) have been deposited onto (110) $DyScO_3$ single crystal substrates at 650°C by molecular beam epitaxy[14,15]. A continuous flux of molecular oxygen mixed with 10% ozone was controlled to yield a background pressure of 5.0×10^{-7} Torr. The average incident flux of both the Sr and Ti sources was maintained constant at 1.0×10^{14} $cm^{-2}s^{-1}$ to achieve a layer-by-layer growth of Sr and Ti in a sequential manner. Reflection high-energy electron diffraction (RHEED) intensity oscillations were used to adjust the stoichiometry of the Sr and Ti molecular beams and ensure that a complete monolayer of each cation was deposited in each shuttered cycle (*i.e.*, 6.6×10^{14} atoms-cm^{-2} of the monolayer doses). X-ray diffraction (XRD), scanning electron microscopy (SEM), and atomic force microscopy (AFM) were used for film structure and surface morphology characterization.

Interdigitated capacitors (IDC) with gaps from 6 to 12 μm were deposited on top of the films through a polymethylmethacrylate (PMMA) lift-off mask by e-beam evaporation of 1.5 μm thick Ag with an adhesive thin layer of Cr and a protective thin layer of Au. The microwave dielectric properties, capacitance and device Q of the ferroelectric thin films, were measured as functions of frequency (45 MHz to 20 GHz) and dc bias voltage (-40 V to 40 V). S_{11} measurements were made using interdigitated capacitors probed by a 200μm pitch Picoprobe microwave probe, which was connected to an HP 8510C network analyzer. The measured S_{11} data were fitted to a parallel resistor-capacitor model to determine capacitance and device Q of the films. The dielectric constant of the films was extracted from the device capacitance and the IDC capacitor dimensions through a conformal mapping technique[16].

3. Results and discussion

3.1. Film structure and surface morphology

Figure 1 shows θ-2θ XRD scans for $Ba_{0.6}Sr_{0.4}TiO_3$ thin films (∼3000Å-thick) deposited onto (100) MgO single crystalline substrates by PLD at 750°C and 200 mTorr O_2 under three different processing conditions;

i) without a buffer layer [Fig. 1a],
ii) with a nominal 200Å-thick BST buffer layer [Fig. 1b] and
iii) with a nominal 600Å-thick BST buffer layer [Fig. 1c].

The BST films in Fig. 1a and 1b can be considered as predominantly (100) oriented films if their diffraction intensities are compared to those of randomly oriented powder diffraction peaks [17]. From an analysis of the XRD data [13], the in-plane lattice parameter of a BST thin film deposited directly on a (001) MgO substrate without a BST buffer layer is observed to be 0.2% larger than the normal lattice parameter, resulting in an in-plane tetragonal lattice distortion ($a_{||} > a_{\perp}$). In comparison, the in-plane lattice parameter of a BST thin film with a nominal 200Å-thick BST buffer layer is observed to be 0.2% smaller than the normal lattice parameter, resulting in a normal tetragonal lattice distortion ($a_{||} < a_{\perp}$), although the structure for the corresponding bulk BST should be a cubic at room temperature. An analysis of the XRD pattern of Fig. 1c indicates the BST thin film deposited with a 600Å-thick BST buffer layer is of a single perovskite phase but does not have a preferred orientation. The ratio of peak intensities of Fig. 1c is very close to the corresponding powder diffraction pattern, indicating that this BST thin film is in a randomly oriented polycrystalline phase. The lattice structure of this BST film was determined to be a cubic phase (a_o=3.966 Å) by analyzing five XRD reflection peaks from the BST film using a least square method, indicating that strain in the BST films with a 600Å-thick BST buffer layer is effectively relieved.

Figure 2 shows SEM images of BST films

(a) without a buffer layer,
(b) with a 200Å-thick BST buffer layer,

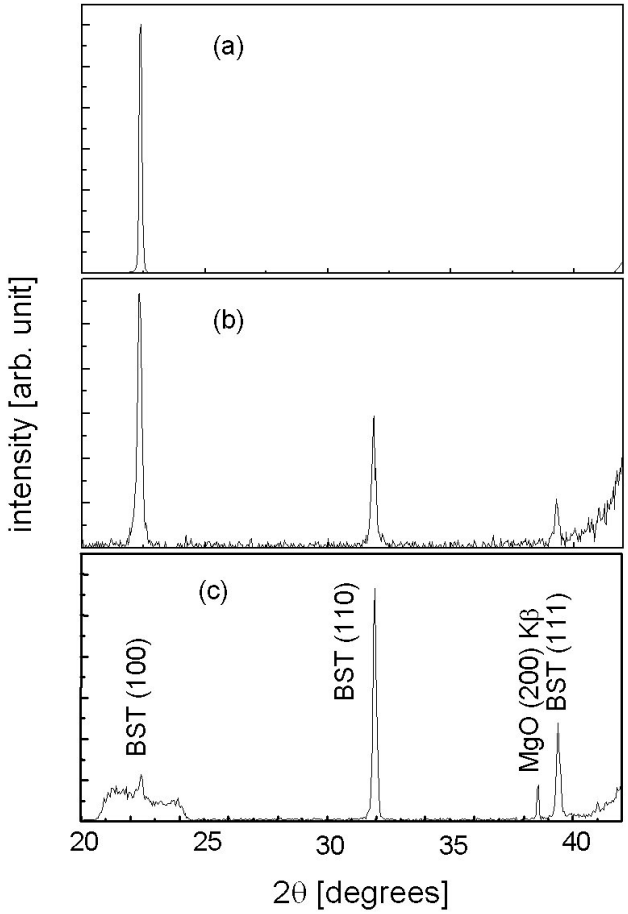

FIGURE 1. XRD patterns of BST thin films deposited on (001) MgO (a) without a buffer layer, (b) with a 200Å-thick BST buffer layer, and (c) with a 600Å-thick BST buffer layer.

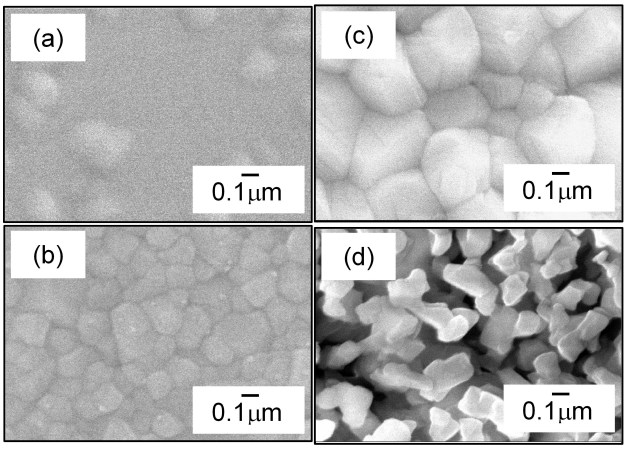

FIGURE 2. SEM images of BST films (a) without a buffer layer, (b) with a 200Å-thick BST buffer layer, (c) with a 600Å-thick BST buffer layer, and (d) fully crystalline BST buffer layer.

(c) with a 600Å-thick BST buffer layer, and

(d) a fully crystalline BST buffer layer.

The buffer layer shown in Fig. 2d shows relatively large voids among the randomly oriented BST grains, and presumably could serve as seeds for the subsequently deposited crystalline BST film. The random orientation of the grains and the voids among the grains in the buffer layer could help to not only relieve film strain effectively but also yo grow crystalline grains significantly (*i.e.*, up to a size of $\sim 0.5\mu$m) in the subsequently deposited film.

Figure 3 shows a θ-2θ XRD scan for $SrTiO_3$ thin film (1000Å-thick) deposited onto (110) $DyScO_3$ single crystal substrates at 650°C by MBE. As shown in the figure, the normal direction to the surface of the $SrTiO_3$ films is only [001] $SrTiO_3$. Also, a Ag/Au peak from the electrodes deposited onto the film appears in the XRD pattern. For these [001]-oriented $SrTiO_3$ films (100, 200, 300, 500, and 1000Å-thick), the lattice parameters along the surface normal ($a_\perp$), and in the plane of the films ($a_{||}$) were determined from XRD patterns of symmetric (004) and asymmetric (024) reflections.

The lattice parameters of the $SrTiO_3$ thin films calculated from an analysis of the XRD data show that the in-plain lattice parameter of $SrTiO_3$ films is extended ($\sim$1% strain for 200, 300, 500, and 1000Å-thick films), and the normal lattice parameter is compressed from the 3.905Å value of bulk $SrTiO_3$[18]. $DyScO_3$ crystal substrate is an $LnMO_3$ orthorhombic structure (Pbnm)[19,20] with anisotropic dielectric properties[14]. It should also be noted that the in-plane lattice parameters,a and b, of pseudocubic $DyScO_3$ substrate are expected to be 3.940Å and 3.943Å, which are $\sim$1% lattice mismatch from the 3.905Å value of bulk $SrTiO_3$.

Figure 4 shows an AFM image of $SrTiO_3$ films (200Å-thick). The film surface is extremely smooth with a surface RMS roughness of 3.880Å, which is approximately the same as one unit cell of the $SrTiO_3$ film with a grain size of about 400$\sim$500Å. Figure 4 is also a typical AFM image for other $SrTiO_3$ films (*i.e.*, 300, 500, and 1000Å-thick).

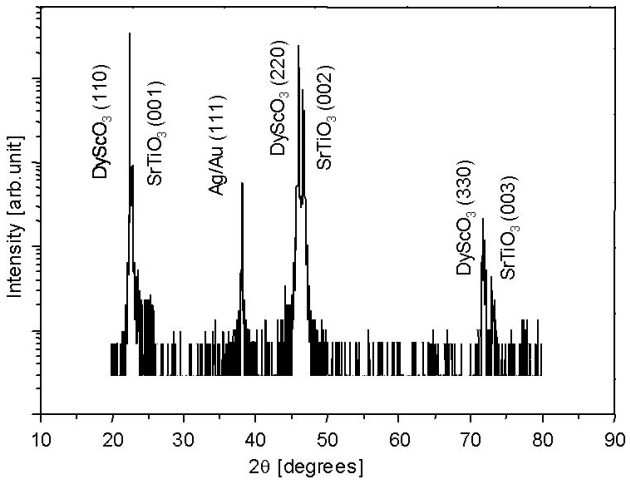

FIGURE 3. XRD pattern of $SrTiO_3$ thin film (1000Å-thick) deposited on (110) $DyScO_3$ substrate.

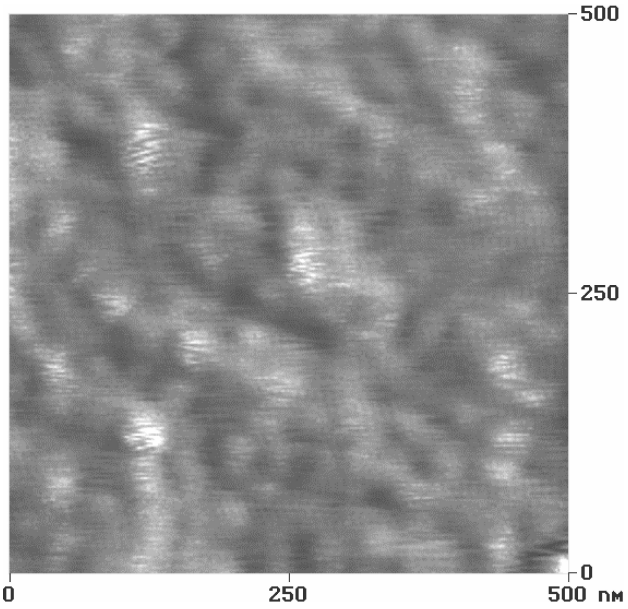

FIGURE 4. AFM image of $SrTiO_3$ film (200Å-thick).

It is worth to note that the severely strained (*i.e.*, $\sim$1%) $SrTiO_3$ films are still in an elastic region without any fracture even though $\sim$1% strain is normally known as a fracture strain for oxide materials.

3.2. Microwave dielectric properties

Figure 5 shows the dielectric tuning of capacitance (C), defined as [C(0)$-$C(V_{DC})]/C(0), and dielectric Q (=1/tanδ) of strained ($a_{||} > a_\perp$ and $a_{||} < a_\perp$) and strain-relieved BST thin films at 8 GHz as a function of applied DC electric field. Typical in-plane film dielectric constants for $a_{||} > a_\perp$ strained, strain-relieved, and $a_{||} < a_\perp$ strained BST thin films were observed to be 800, 500, and 300, respectively. The strain-relieved BST films exhibit a relatively high dielectric Q_{0V} ($\sim$100) with a reasonably good dielectric tuning ($\sim$20%

at 20 V/μm). The strained BST films show either high dielectric tuning ($\sim$ 50% at 25 V/μm) with a low dielectric Q_{0V} ($\sim$20) or high dielectric Q_{0V} (>150) with a low dielectric tuning $\sim$ 5% at 25 V/μm), depending on the film strain, $a_{||} > a_{\perp}$ or $a_{||} < a_{\perp}$, respectively.

Figure 6 shows the dielectric constant of $SrTiO_3$ thin films (500Å-thick) as a function of applied dc bias measured at 10GHz and room temperature. The as-deposited $SrTiO_3$ film exhibits a huge dielectric constant (*i.e.*, $\sim$6000) and a large dielectric tuning (*i.e.*, $\sim$85% with a 4V/μm) at room temperature. This has never been reported before for the room temperature dielectric properties of $SrTiO_3$, in either bulk and thin film form. It is also interesting to note that most of the dielectric tuning of as-deposited $SrTiO_3$ film occurs at a low dc bias field (*i.e.*, $\sim$75% with a 1V/μm). As shown in Fig. 6, the annealing effect is critical on the dielectric properties as the annealed film (*i.e.*, for 30 min at 700°C in atmosphere) shows a significantly reduced dielectric constant and dielectric tuning.

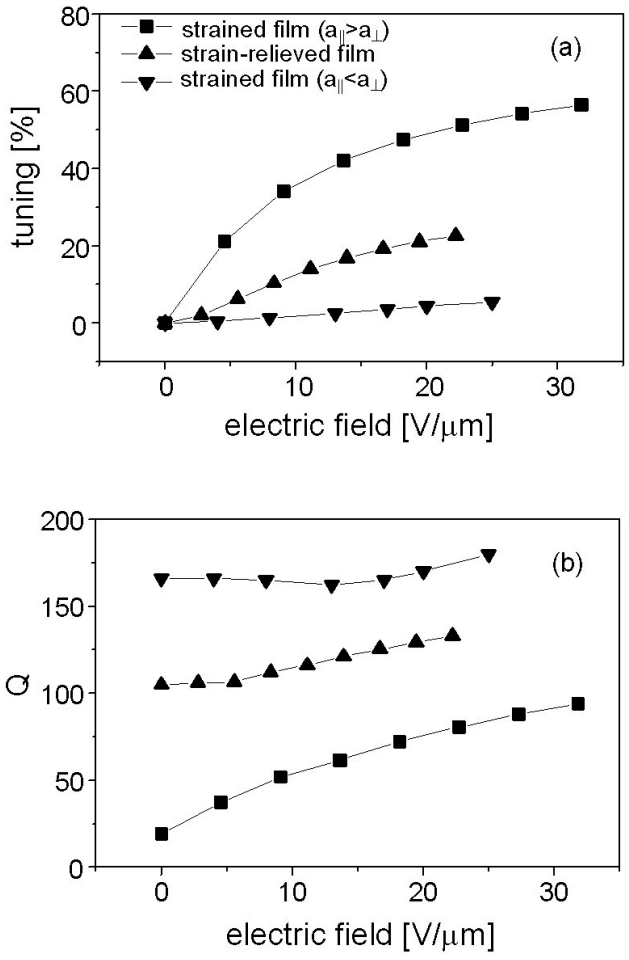

FIGURE 5. (a) Dielectric tuning and (b) dielectric Q of strained, and strain-relieved BST thin films at 8 GHz as a function of applied DC electric field.

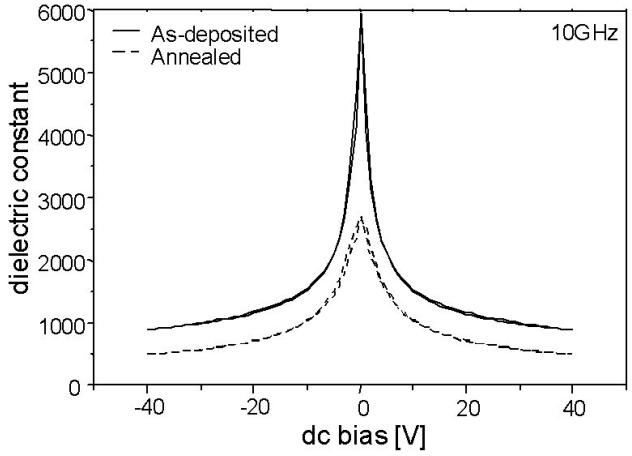

FIGURE 6. Room temperature dielectric constant of $SrTiO_3$ thin films (500Å-thick) at 10 GHz.

Figure 7 shows the capacitance and device Q of annealed $SrTiO_3$ films (500Å-thick) as a function of temperature and dc bias (*i.e.*, 0V for solid lines and 40V for dotted lines) measured at 10GHz. As shown in the figure, the ferroelectric transition appears at 285K and 290K for annealed and as-deposited 500Å-thick film, respectively, which are just below room temperature. This is why the $SrTiO_3$ films exhibit abnormal nonlinear dielectric properties with a high dielectric constant and dielectric tuning at room temperature as shown in Fig. 6. Also, the phase transition peak for as-deposited 500Å-thick film (*i.e.*, 290K) is observed to shift to a lower temperature (*i.e.*, 285K) after the annealing process (Fig. 7). This is the reason that the as-deposited $SrTiO_3$ film shows a higher dielectric constant and dielectric tuning than the annealed $SrTiO_3$ film at room temperature (Fig. 6). Even though it is not clear why the phase transition peak for the annealed film appears at a lower temperature, presumably it is due to the possible annealing effects such as relaxed film strain and reduced oxygen vacancies, which are expected to cause a reduced in-plane lattice constant.

A typical device Q at 0V dc bias of $SrTiO_3$ films shows a maximum value of 30 to 40 at a 110K and a minimum value of 10 to 20 at a 275K, which is associated with the phase transition peak. The device Qs of the films, which look too low to be applied to real devices, is believed to be mostly due to the dielectric Q (= 1/tanδ) because any other loss factors (*i.e.*, electrode conduction, leakage current, and substrate dielectric) are expected to be much lower compared to the dielectric loss in the film. Presumably, the relatively low dielectric Qs (*i.e.*, high dielectric losses) of the $SrTiO_3$ films is due to the film strain and well-oriented film microstructure (*i.e.*, epitaxy). This is because the total electric polarization in the film depends on the magnitude of the dipole moment formed in the unit cell, which is associated with film strain, and the coupling of each dipole with each other, which is related to film orientation. Therefore, the relatively high dielectric loss of the strained epitaxial $SrTiO_3$ films must be related to the motion of the resulting large dipole moments with RF signal.

Previously, we reported a theoretical analysis of the dielectric properties of epitaxial BST films[11] based on Devonshire's phenomenological theory[21]. Figure 8 shows a theoretical phase transition peak as a function of film strain with some measured data of the $SrTiO_3$ films. The theoretical expression between the phase transition peak, T_C, and the film strain, x, (*i.e.*, in-plane strain for our measurement configuration) can be easily derived from the previous report. It is included in the figure and the relevant parameters can be found elsewhere[11]. As shown in the figure, the phase transition peak can be well predicted as a function of film strain if the strain measurements show a better accuracy.

Further work will be performed to elucidate the film strain effect on the tunable microwave dielectric properties by a direct film strain-microwave property measurement. Through the novel direct measurements, it is expected to answer to many unknowns about the microwave properties of strained ferroelectric thin films.

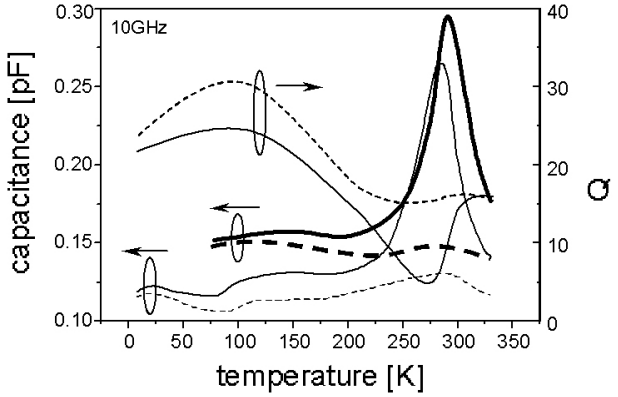

FIGURE 7. Capacitance and dielectric Q of annealed $SrTiO_3$ thin film (500Å-thick) as a function of temperature, and dc bias voltages (0V for lines and 40V for dot lines) at 10GHz (also, the capacitance of as-deposited film is plotted with thicker lines).

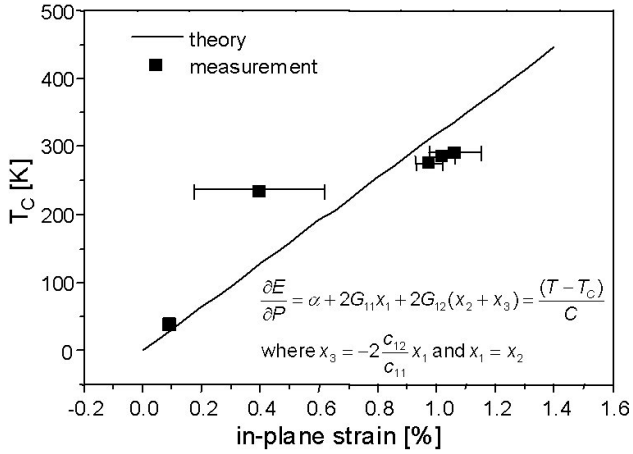

FIGURE 8. Theoretical phase transition peak as a function of film strain, and several measurement data (one of the measurement data (*i.e.*, T_C= 35 K with 0.1% film strain for $SrTiO_3$ film on (001)MgO) is included from our previous work).

4. Summary

Strain-relieved BST films are observed to show the dielectric properties by exhibiting a significantly high dielectric Q (=1/tanδ >100) while retaining a useful dielectric tuning (=[C(0)-C(23V/μm)]/ C(0) >20 %, where C is the film capacitance) at 8 GHz compared to strained BST thin films. Strain-enabled films can be designed to have suppressed or enhanced unit cell polarization (depending on the compressed or elongated unit cell), which results in significantly low dielectric loss or high dielectric tuning, respectively. The room temperature dielectric constant and tuning of significantly strained (*i.e.*, $\sim$1%) STO films are observed to be 6000 and 75% with a 1V/μm at 10 GHz, respectively.

1. C.H. Mueller, R.R. Romanofsky, and F.A. Miranda, *IEEE Potentials* **20** (2001) 36.
2. S.S. Gevorgian and E.L. Kollberg, *IEEE Trans. Microwave Theory Tech.* **49** (2001) 2117.
3. D.S. Korn and H.-D. Wu, *Integrated Ferroelectrics* **24** (1999) 215.
4. W.J. Merz, *Phys. Rev.* **78** (1950) 52.
5. J.C. Slater, Phys. Rev. **78** (1950) 748.
6. P.W. Forsbergh J$_R$., *Phys. Rev.* **93** (1954) 686.
7. G.A. Samara and A.A. Giardini, *Phys. Rev.* **140** (1965) A954.
8. T. Schimizu, *Solid State Comm.* **102** (1997) 523.
9. N.A. Pertsev, A.G. Zembilgotov, and A.K. Tagantsev, *Phys. Rev. Lett.* **80** (1998) 1988.
10. W. Chang, J.S. Horwitz, J.M. Pond, S.W. Kirchoefer, and D.B. Chrisey, *Materials Research Society Symposium Proceedings* **526** (1998) 205.
11. W. Chang *et al.*, Integr. Ferroelectr. **24** (1999) 257.
12. N.A. Pertsev, A.K. Tagantsev, and N. Setter, *Phys. Rev. B* **61** (2000) R825.
13. W. Chang, S.W. Kirchoefer, J.M. Pond, J.S. Horwitz, and L. Sengupta, *J. of Appl. Phys.* **92** (2002) 1528.
14. J.H. Haeni and D.G. Schlom (private commucation).
15. J.H. Haeni, C.D. Theis, and D.G. Schlom, *J. Electroceram.* **4** (2000) 385.
16. S.S. Gevorgian, T. Martinsson, P.I.J. Linner, and E.L. Kollberg, *IEEE Trans. Microwave Theory Tech.* **44** (1996) 896.
17. *X-ray diffraction JCPDS #34-0411 for $Ba_{0.6}Sr_{0.4}TiO_3$.*
18. W. Chang *et al.* (to be submitted)
19. J.A.W. Dalziel, *J. Chem. Soc.* (1959) 1993.
20. *X-ray diffraction JCPDS #27-0204 for $DyScO_3$.*
21. A.F. Devonshire, *Adv. in Phys.* **3** (1954) 85.